
18 Eigenvalue communications in nonlinear fiber channels

Jaroslav E. Prilepsky and Sergei K. Turitsyn

Continuous progress in optical communication technology and corresponding increasing data rates in core fiber communication systems are stimulated by the evergrowing capacity demand due to constantly emerging new bandwidth-hungry services like cloud computing, ultra-high-definition video streams, etc. This demand is pushing the required capacity of optical communication lines close to the theoretical limit of a standard single-mode fiber, which is imposed by Kerr nonlinearity [1–4]. In recent years, there have been extensive efforts in mitigating the detrimental impact of fiber nonlinearity on signal transmission, through various compensation techniques. However, there are still many challenges in applying these methods, because a majority of technologies utilized in the inherently nonlinear fiber communication systems had been originally developed for linear communication channels. Thereby, the application of “linear techniques” in a fiber communication systems is inevitably limited by the nonlinear properties of the fiber medium. The quest for the optimal design of a nonlinear transmission channels, development of nonlinear communication techniques and the usage of nonlinearity in a “constructive” way have occupied researchers for quite a long time. For instance, the idea of balancing the nonlinear self-phase modulation effect by dispersion (or vice versa) using soliton pulses was proposed by Hasegawa and Tappert in the early 1970s [5], when intensity modulation and direct detection were the main technology trend [6–9]. The relevant advances in this technique include ultra-long wavelength-division-multiplexing soliton transmission, dispersion-managed solitons and many other interesting methods (see [6–11] and references therein). However, in the past decade traditional soliton approaches lost their appeal due to fast progress in various other (simpler implementation) transmission techniques. Moreover, increasing symbol rates stipulate the use of shorter pulses, which, for solitons with power inversely proportional to pulse width, means increasingly substantial nonlinear interactions and pattern dependent jitter effects. Recently, modification of soliton techniques to the coherent detection system was proposed [12–14], with the first studies indicating a decent potential for this approach. In general, currently there is an evident need for radically different approaches to coding, transmission, and processing of information in fiber communication channels that would take into account the nonlinear properties of optical fiber, allowing one to overcome the limits of linear techniques.

More than 20 years ago Hasegawa and Nyu [15] (see also Chapter 4.4. of the monograph by Hasegawa and Kodama [7]), considering the nonlinear Schrödinger equation (NLSE) as a model for signal propagation in a single-mode fiber, put forward the idea of exploiting the *nonlinear spectrum* of a signal for the purposes of information transmission. Since then, this concept has been known as “eigenvalue communications” because the authors proposed encoding information using special discrete eigenvalues (non-dispersive part of the nonlinear spectrum), which correspond to solitonic degrees of freedom and have no analogues in linear problems. This proposal is an example of a fundamentally nonlinear communication technique based on the unique property of the channel – the *integrability* of the corresponding nonlinear channel model given by the NLSE [16]. Currently, this prefiguring idea of using the nonlinear spectrum in data encoding, processing and transmission processes, is generally understood in a somewhat wider sense, and can be formulated as follows. In linear communication channels, spectral components (modes) defined by the Fourier transform (FT) of the signal propagate without interactions with each other. In certain nonlinear channels (*integrable channels*), such as the one governed by the NLSE, there exist nonlinear modes (nonlinear signal spectrum) that also propagate without interacting with each other and without corresponding nonlinear cross-talk, effectively, in a linear manner. Thus the parameters of these nonlinear modes can be used for encoding and efficient transmission of the information over a nonlinear fiber, the signal propagation inside which can be well modeled (at least in the leading approximation) by an integrable equation, for instance, by the NLSE.

The transition from the true space-time domain into the nonlinear spectral domain and back is achieved by performing the so-called *nonlinear Fourier transform* (NFT) — a technique introduced in the 1970s [16–19]. NFT operations constitute nothing more than the core parts of the general inverse scattering transform (IST) method [20, 21] for the solution of initial-value problems associated with integrable evolutionary equations and, in particular, developed for the the solution of the NLSE by Zakharov and Shabat in [16], and, further, for the so-called Manakov system, relevant to optical signal transmission using polarization degrees of freedom, by Manakov [22]. It should be noted that until recently the potential of the original idea expressed in [15], namely, the usage of the specifically nonlinear quantities from the IST method for the signal processing and transmission, had been largely overlooked by the communications and engineering community, although pulse-to-soliton conversion and soliton evolution problems were being widely studied by physicists in a number of different areas. Only recently this concept has attracted a new wave of attention with application to signals transmission and processing, highlighting the re-emergence of the eigenvalue communications [23–34]. Over the past few years several groups have revisited and extended the original ideas of Hasegawa and Nyu in the context of coherent optical communications. The concept itself is being approached from two somewhat

“orthogonal and complementary” pathways, neither of which excludes the parallel implementation of the alternative approach. These two main directions in “eigenvalue communication” methodology can be categorized according to what part of the nonlinear spectrum is used for modulation and transmission. The first approach involves the use of discrete eigenvalues and related solitonic quantities for signal transmission [15, 27–29, 34] and processing [26, 30], where the reported spectral efficiency of the method reached a decent value of more than 3 bit/sec/Hz [31]. The second method has been pursued by the Aston group and collaborators: it deals with the modulation of the continuous part of the nonlinear spectrum for signal encoding and efficient transmission in optical fibers [24, 25, 32, 33]. In this chapter we review the present state of this completely new direction in “eigenvalue communications” following recent publications [24, 25, 32, 33].

18.1 INTRODUCTION AND MAIN MODEL DESCRIPTION

Optical fiber systems form the backbone of global telecommunication networks and currently carry the majority of the world’s information traffic, with the “fifth generation” of optical transmission systems operating with advanced modulation formats, e.g., orthogonal frequency division multiplexing (OFDM), digital signal processing techniques, etc. Skyrocketing demand for communication speed is exerting great pressure on the networks’ infrastructure at every scale, which explains the real motivation behind the overwhelming part of optical communications research. Since the introduction of fiber-optic communications in the late 1970s, many technological advances, such as erbium-doped fiber amplifiers (EDFA), wavelength division multiplexing (WDM), dispersion management, forward error correction, and Raman amplification, have been developed to enable the exponential growth of data traffic [1, 2, 6]. The introduction of advanced modulation formats and digital signal processing for coherent communications led to practical implementation of systems with 100 Gb/sec channel rates. The key to this breakthrough is the possibility of mitigating the most important linear transmission impairments, such as fiber link dispersion and polarization mode dispersion. In coherent fiber optic communication systems, the received optical signal is digitized through high-speed analog-to-digital converters and then processed using digital signal processing (DSP) algorithms. The input signal is then recovered with the accuracy allowed by the channel noise and the transmission effects that are not equalized by the DSP. After the mitigation of linear effects, noise and nonlinear impairments become the key factors in limiting the performance of coherent fiber optic communication systems.

In recent years, a number of techniques have been introduced and studied for surmounting the capacity limit (occurring due to Kerr nonlinearity) through various nonlinearity compensation techniques, including digital back-propagation (DBP) [35], optical phase conjugation [36], and phase-conjugated twin waves [37], to mention a few recent advances. However, there are still many limitations in applying the aforementioned nonlinear

compensation methods. A significant step forward would take place if a method could “incorporate” fiber nonlinearity constructively when designing core optical communication coding, transmission, detection, and processing approaches. It actually means that the true capacity limits of nonlinear fiber channels have yet to be found.

In general, the power of a signal transmitted through an optical fiber link is degraded by loss and has to be periodically recovered through optical amplification. In many important practical situations, the averaging of such periodic loss and gain results in an effectively lossless propagation model – the NLSE [6–8, 10, 11], which describes the continuous interplay between dispersion and nonlinearity. Moreover, using technology developed at Aston University, it was demonstrated experimentally that fiber loss can be compensated continuously along a fiber span, leading to effectively quasi-lossless transmission [38–42]. Overall, the NLSE can be considered a principal master model for demonstrating key techniques and approaches in optical fiber communications. Written for a complex slow-varying optical field envelope $q(z, t)$, it reads as (so far we disregard all deviations from the pure integrable case)

$$i q_z - \frac{\beta_2}{2} q_{tt} + \gamma q |q|^2 = 0, \quad (18.1)$$

where z stands for the propagation distance and t is the time in the frame co-moving with the group velocity of the envelope. Depending on the sign of the group velocity dispersion coefficient β_2 , two physically different situations are generally considered with regard to model (18.1): (i) the case of anomalous dispersion, where the dispersion coefficient $\beta_2 < 0$, resulting in the so-called *focusing* NLSE, and (ii) the normal dispersion case with $\beta_2 > 0$, corresponding to the *defocusing* type of the NLSE (the higher-order dispersion terms are not considered). The instantaneous Kerr nonlinearity coefficient γ is expressed through the nonlinear part of refractive index n_2 and an effective mode area A_{eff} : $\gamma = n_2 \omega_0 / c A_{eff}$, with c being the vacuum speed of light and $\omega_0 = 2\pi\nu_0$ being the carrier frequency of the envelope $q(t, z)$. Further, we will use the explicit form of the NFT operations attributed to the the normalized versions of the NLSE. We normalize time in Eq. (18.1) to the characteristic time related to an input signal T_s , which can be, e.g., the extent of the RZ signal or the characteristic duration of a single information-bearing symbol (the normalization value T_s is rather a matter of convenience), and then use the effective z -scale associated with T_s : $Z_s = T_s^2 / |\beta_2|$. Then, we measure the power of the input in units of $P_0 = (\gamma Z_s)^{-1}$ and normalize the signal amplitude correspondingly. The summary of normalizations is

$$\frac{t}{T_s} \rightarrow t, \quad \frac{z}{Z_s} \rightarrow z, \quad \frac{q}{\sqrt{P_0}} = q \sqrt{\gamma Z_s} \rightarrow q. \quad (18.2)$$

For the anomalous dispersion case, the typical value of β_2 is $-22 \text{ ps}^2/\text{km}$, and for normal dispersion we use the value $\beta_2 = 5 \text{ ps}^2/\text{km}$; the typical value of the Kerr coefficient is $\gamma = 1.27 \text{ (W}\cdot\text{km)}^{-1}$.

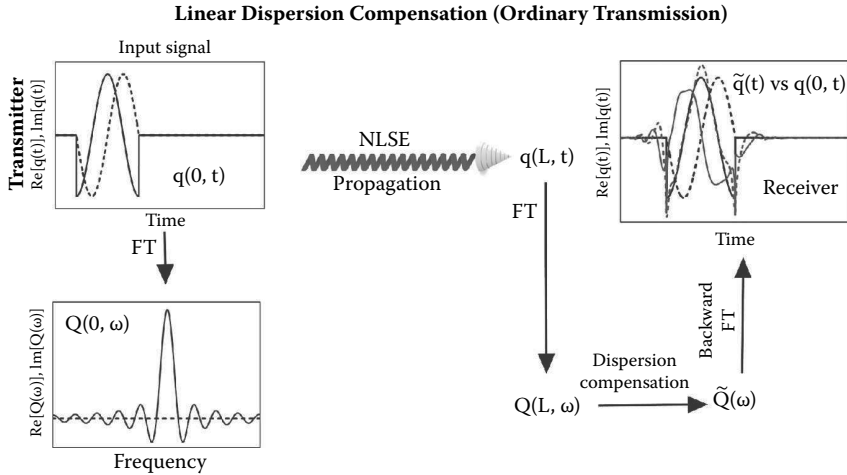


FIGURE 18.1: Flowchart of the linear scheme (chromatic dispersion compensation), valid for both signs of dispersion.

Later we will compare the results of the different NFT-based schemes against the linear dispersion compensation technique, given schematically in Fig. 18.1. For the NLSE, at a very low signal power the digital compensation of dispersion produces perfect recovery of the initial signal (when noise is not taken into account). However, when signal power gets higher, the compensation of dispersion recovers the initial signal, leaving noticeable corruption of the post-processed received waveform (depending on the input power level and propagation distance) even without taking into account the channel noise; see the insets of Fig. 18.1.

In addition to a fiber’s dispersion and nonlinearity, the key master model that describes the signal propagation in a fiber link takes into account the effect of noise. The noise term results from amplifier spontaneous emission (ASE) either from the EDFAs (in the path average model) or from the distributed Raman amplification (see for details references and discussion in [1]):

$$iq_z - \frac{\beta_2}{2}q_{tt} + \gamma q|q|^2 = \Gamma(t, z). \tag{18.3}$$

The random complex quantity $\Gamma(t, z)$ describes noisy corruptions due to the ASE: It is generally written as a symmetric additive complex Gaussian white noise (AWGN) with zero average, fully characterized by its autocorrelation intensity:

$$\langle \Gamma(t, z)\bar{\Gamma}(t', z') \rangle = 2D \delta(t - t') \delta(z - z'),$$

where the overbar stands for the complex conjugation. Reference [1] provides a detailed account of how noise intensity D relates to the parameters of the line.

It is well known that the NLSE (without perturbation) belongs to the class of integrable nonlinear systems [7, 8, 10, 16–21]. In particular, this means

that the focusing NLSE possesses a special type of solution: highly robust localized nonlinear waves, called solitons. However, it should be stressed that the methodology of eigenvalue communication is conceptually different from pure soliton-based transmission [12–14], even though the solitonic components can actually be present in the transmitted pulse: The information carriers there are not the soliton waveshapes themselves, but the IST data attributed, in particular (but not necessarily), to the solitonic degrees of freedom. This fact indicates the momentous difference between soliton-based transmission and eigenvalue communication.

18.2 NONLINEAR FOURIER TRANSFORM ASSOCIATED WITH NLSE

One of the particular manifestations of the integrability property is that, given the initial conditions (in the context considered, the waveform of the input signal), we can propagate the signal to a distance $z = L$ in three steps, which have direct analogies with the same stages in the consideration of linear problems, although the immediate implementation of these steps differs significantly from the linear case.

1. The first step is the mapping of the input profile to the spectral domain. For a linear channel, this operation corresponds to the ordinary forward Fourier transform (FT), and we will call this stage the *forward NFT* (FNFT), by analog with the linear situation. For nonlinear propagation, this stage involves solving the specific direct scattering problem associated with an integrable equation and produces a set of *scattering data*, where the particular quantities (continuous spectrum and a set of discrete complex eigenvalues, if the latter exists) are then associated with orthogonal nonlinear “normal modes.”
2. The next step is the propagation of the initial spectral distribution (again, a continuous spectrum and complex eigenvalues) to distance L : Here, in both linear and nonlinear cases, the spectrum evolves according to the linear dispersion law. So, a further impetus for an analogy between NFT and its linear counterpart is that the former does to NLSE what the latter does to the linear equations: just as the linear FT changes dispersion to a phase rotation in frequency space so the NFT leads to a trivial phase rotation of the spectral data. This means that the fiber nonlinear transmission effects are effectively included in the NFT.
3. The last stage is the recovery of the solution profile in the space-time domain: It is the backward FT in the linear case. For the nonlinear integrable problem, the backward NFT (BNFT) amounts to the solution of the so-called Gelfand–Levitan–Marchenko equations, and this step accomplishes the finding of a solution (signal profile) at distance L . These three stages, which provide the solution of a nonlinear equation at distance L , constitute the essence of the IST method.

References [7, 16–21] provide numerous details, examples and profound explanation of the IST method, and below we briefly present only some relevant parts of this.

18.2.1 FORWARD NONLINEAR FOURIER TRANSFORM (ZAKHAROV–SHABAT DIRECT SCATTERING PROBLEM) FOR THE FOCUSING NLSE

In this subsection we consider the FNFT attributed to the anomalous dispersion (focusing) case, where the normalized NLSE (18.1) is explicitly rewritten as

$$iq_z + \frac{1}{2}q_{tt} + q|q|^2 = 0. \tag{18.4}$$

The FNFT operation for Eq. (18.4) requires solutions of the so-called Zakharov–Shabat spectral problem (ZSSP), which corresponds to the scattering problem for a non-Hermitian (for the anomalous dispersion) Dirac-type system of equations for two auxiliary functions $\phi_{1,2}(t)$, with the NLSE input waveform $q(0, t) \equiv q(t)$ serving as an effective potential entering the equations

$$\frac{d\phi_1}{dt} = q(t)\phi_2 - i\zeta\phi_1, \quad \frac{d\phi_2}{dt} = -\bar{q}(t)\phi_1 + i\zeta\phi_2. \tag{18.5}$$

Here, ζ is a (generally complex) spectral parameter, $\zeta = \xi + i\eta$, and the potential $q(t)$ is supposed to decay as $t \rightarrow \pm\infty$ (see the specific constraints imposed on $q(t)$ decay in [16–21]).

At the left end $t \rightarrow -\infty$ we fix the “initial” condition for the incident wave scattered by the potential $q(t)$ to have the so-called Jost solution $\vec{\Phi}(t, \zeta) = [\phi_1(t, \zeta), \phi_2(t, \zeta)]^T$:

$$\vec{\Phi}(t, \zeta) \Big|_{t \rightarrow -\infty} = \begin{pmatrix} 1 \\ 0 \end{pmatrix} \exp(-i\zeta t).$$

With this initial condition, at the right end, $t \rightarrow +\infty$, we define two Jost scattering coefficients, $a(\zeta)$ and $b(\zeta)$, constituting the essence of the FNFT:

$$a(\zeta) = \lim_{t \rightarrow \infty} \phi_1(t, \zeta), \exp(i\zeta t), \quad b(\zeta) = \lim_{t \rightarrow \infty} \phi_2(t, \zeta) \exp(-i\zeta t), \tag{18.6}$$

with $\phi_{1,2}$ being the corresponding elements of vector $\vec{\Phi}(t, \zeta)$. The (right) reflection coefficient associated with Eq. (18.5) is then defined as

$$\rho(\xi) = \frac{b(\xi)}{a(\xi)} = \lim_{t \rightarrow \infty} \frac{\phi_2(\xi, t)}{\phi_1(\xi, t)} \exp(-2i\xi t). \tag{18.7}$$

The FNFT operation corresponds to the mapping of the initial field, $q(0, t) = q(t)$, onto the set of *scattering data*:

$$\Sigma = \left[\rho(\xi), \xi \in \mathbb{R}, \quad \left\{ \zeta_n, C_n \equiv \frac{b(\zeta_n)}{a'(\zeta_n)} \right\} \right], \tag{18.8}$$

Downloaded by [Aston University] at 01:44 14 December 2016

where index n runs over all discrete eigenvalues of ZSSP, Eq. (18.5) (if these are present). The quantity $\rho(\xi)$ from Eqs. (18.7) and (18.8) defined for real ξ (“frequency”) plays the role of continuous nonlinear spectral distribution, while the quantities associated with discrete eigenvalues describe solitonic degrees of freedom and do not have analogs in linear problems. The evolution of the reflection coefficient is given by

$$\rho(L, \xi) = \rho(\xi) \exp(2i\xi^2 L), \quad (18.9)$$

where $\rho(L, \xi)$ is the value of the coefficient after propagation to the distance L . From Eq. (18.9), one can see that the nonlinear spectrum obeys the linear dispersion law of the NLSE (18.4) if one associates the linear frequency ω with the quantity ξ as $\xi = -\omega/2$. Indeed, from the IST theory, it is known [17] that asymptotically in the linear limit the following formula is valid:

$$\rho(\xi) \Big|_{|q(t)| \rightarrow 0} = -\bar{Q}(-2\xi), \quad (18.10)$$

where $Q(\dots)$ identifies the linear FT of the signal $q(t)$. In view of Eq. (18.10), it is useful to define the *nonlinear spectral function* (NSF) $N(\omega)$ associated with $\rho(\xi)$ via

$$N(\omega) = -\bar{\rho}(\xi) \Big|_{\xi = -\frac{\omega}{2}}. \quad (18.11)$$

So, in the linear limit the NSF (18.11) coincides with the linear spectrum of the signal $q(t)$.

Quite often for the sake of computation convenience the *left set* of scattering data is defined for Eq. (18.5); as for the linear FT, one can use different signs in the transform exponent. In particular, the left reflection coefficient on the real axis is given by

$$r(\xi) = \frac{\bar{b}(\xi)}{a(\xi)}. \quad (18.12)$$

Obviously, the poles of the left reflection coefficient (18.12) coincide with those of the right one, Eq. (18.7), as in both cases these are defined by $a(\zeta) = 0$ in the upper complex half-plane of spectral parameter ζ . The quantities C_n (norming constants) from (18.8) change to $\bar{C}_n = [b(\zeta_n) a'(\zeta_n)]^{-1}$. Generally, the definitions of the complete set of scattering data through the right and left sets are equivalent, leading to unique recovery of the profile in the time domain, and we refer an interested reader to the work by Ablowitz et al. [17], where the IST method is simultaneously formulated in terms of both left and right sets. One of the distinctions is that the evolution law for $r(L, \xi)$ changes the sign in the exponent

$$r(L, \xi) = r(\xi) \exp(-2i\xi^2 L), \quad (18.13)$$

and the definition for the NSF in terms of $r(\xi)$ reads

$$N(\omega) = -r(\xi) \Big|_{\xi = -\frac{\omega}{2}}. \quad (18.14)$$

18.2.2 MODIFICATION OF THE FNFT FOR THE NORMAL DISPERSION CASE

Now consider the case of the normal dispersion NLSE, with the explicit normalized form

$$iq_z - \frac{1}{2}q_{tt} + q|q|^2 = 0. \tag{18.15}$$

The associated ZSSP transforms as follows (cf. Eq.(18.5)):

$$\frac{d\phi_1}{dt} = q(t)\phi_2 - i\xi\phi_1, \quad \frac{d\phi_2}{dt} = \bar{q}(t)\phi_1 + i\xi\phi_2. \tag{18.16}$$

We have already written this ZSSP specifically for real spectral parameter ξ . The significant difference of the focusing case (18.5) from the defocusing ZSSP (18.16) is that the latter is Hermitian. It signifies that for the normal dispersion one cannot have soliton solutions (complex discrete eigenvalues) emerging from any sufficiently localized input. The right and left reflection coefficients are defined in the same manner as in [Subsection 18.2.1](#). Due to the different sign of the dispersion in Eq. (18.15), we also have the change of sign in the evolution law exponent for the reflection coefficient attributed to Eqs. (18.15) and (18.16):

$$r(L, \xi) = r(\xi) \exp(2i\xi^2 L). \tag{18.17}$$

18.2.3 BACKWARD NONLINEAR FOURIER TRANSFORM (GELFAND–LEVITAN–MARCHENKO EQUATION)

The backward NFT maps the scattering data Σ onto the field $q(t)$: This is achieved via the Gelfand-Levitan-Marchenko equations (GLME) for the unknown functions $K_{1,2}(t, t')$. The general form of the GLME written in terms of the left scattering data reads:

$$\begin{aligned} \bar{K}_1(t, t') + \int_{-\infty}^t dy F(t' + y)K_2(t, y) &= 0, \\ \pm \bar{K}_2(t, t') + F(t + t') + \int_{-\infty}^t dy F(t' + y)K_1(t, y) &= 0, \end{aligned} \tag{18.18}$$

$t > t',$

where “+” corresponds to the focusing and “-” to the defocusing NLSE. For the defocusing case (“-” sign) the quantity $F(t)$ can contain both contributions from the solitonic and continuous parts:

$$F(t) = -i \sum_k \tilde{C}_k e^{-i\zeta_k t} + \frac{1}{2\pi} \int_{-\infty}^{\infty} d\xi r(\xi) e^{-i\xi t}. \tag{18.19}$$

Having solved the GLME (18.18) for $K_{1,2}(t, t')$, the solution sought in the space-time domain is recovered as $q(t) = \pm 2\bar{K}_2(t, t)$. However, for the GLME associated with the soliton-free case, considered later in this chapter, this

Downloaded by [Aston University] at 01:44 14 December 2016

expression reduces to the simple FT of $r(\xi)$,

$$F(t) = \frac{1}{2\pi} \int_{-\infty}^{\infty} d\xi r(\xi) e^{-i\xi t},$$

which is valid for both signs of the dispersion. When one is interested in the solution $q(L, t)$, the quantity $r(\xi)$ in (18.19) is replaced with $r(L, \xi)$, given either by Eq. (18.13) or (18.17), depending on the sign of the dispersion. So, the resulting solution of the GLME (18.18) becomes the function of L : $K_{1,2}(L; t, t')$.

18.2.4 SOME REMARKS ON NUMERICAL METHODS FOR COMPUTING NFT AND ASSOCIATED COMPLEXITY

Inasmuch as the form of the FNFT and BNFT operations is seemingly different, numerical methods for the solution of the ZSSP, Eqs. (18.5) and (18.16) and for the GLME (18.18) are also distinct. For the latter we note that for our purposes we do not consider the soliton's contribution.

The well-know methods for the solution of ZSSP involve Crank–Nicolson finite-difference discretization, Ablowitz–Ladik discretization (where the resulting differential-difference NLSE form is also integrable), the Bouffetta–Osborne method [43, 44], where one uses a piecewise-constant approximation of the “potential” $q(t)$, Runge–Kutta integration of the ZSSP [44], the spectral collocation method [26], etc. The methods for the ZSSP are well reviewed in [28, 46]. For solitonic quantities, one has to augment the solving routine with a root finding method, such as the Newton–Raphson method, to locate zeros of $a(\xi)$. This step, in general, can bring about an increase in computational complexity.

For the solution of GLME (18.18), there exists a multitude of methods stemming mostly from the Bragg grating synthesis research, which are applicable in the soliton-free case for both dispersion signs. We mention different peeling algorithms [45] and the Toeplitz matrix based method [33, 47]; see also the references in these works.

At this point it is pertinent to discuss the numerical complexity of the NFT as compared to, say, the popular digital back-propagation (DBP) technique for the removal of nonlinear distortions [35]. In the latter one reads the transmitted waveform at the receiver, inserts it as an input for the noiseless NLSE, Eq. (18.1), and then solves it in a backward direction. The numerical solution of the NSLE is usually performed by using the split-step Fourier method [6, 35], which requires $\sim N_z M_t \log M_t$ floating-point operations (flops), M_t being the number of discretization (sampling) points in the time domain, and N_z the number of steps in z , which grows with the transmission length and can depend on the pulse power. The transmission techniques that we consider further involve either one or two nonlinear transforms, each of those requiring $\sim M_t^2$ flops with the use of the well-developed methods mentioned

above. Even with such an estimate, the complexity of the NIS can be comparable to that of the DBP when $M_t^2 \sim N_z M_t \log M_t$ [25]. However, recent advance in numerical NFT methods indicate that the complexity of the NFT operations can be potentially reduced even further. For the ZSSP, a recent study by Wahls and Poor [46] suggests that the recovery of the *continuous* part of the nonlinear spectrum can be made in only $\sim M_t \log^2 M_t$ flops. For the GLME, in another work by the same authors [48] some arguments in favor of the possibility for the fast BNFT operation with the same order of flops are given. The Toeplitz matrix based GLME solution method [33, 47] can be potentially integrated with the superfast Toeplitz matrix inversion algorithms (see the direct references in [25, 33]), also resulting in overall NFT complexity reductions. Taking these estimations, we believe that NFT-based transmission methods can potentially outperform the DBP and other nonlinearity compensation techniques in terms of numerical complexity for digital signal processing.

18.3 TRANSMISSION USING CONTINUOUS NONLINEAR SPECTRUM – NORMAL DISPERSION CASE

In [24] the case of transmission through the channel described by the normal dispersion NLSE (18.15) was addressed. The normalization parameters were taken as follows: $T_s = 25$ ps, $Z_s = 125$ km. As mentioned in [Subsection 18.2.2](#), for this dispersion sign no solitons can emerge from the input having a localized extent, and this fact greatly simplifies the usage of NFT operations because one does not have to deal with discrete eigenvalues. We call this approach “the straight IST-based method” insofar as in this case the course of actions is completely similar to the linear case; compare Figs. 18.1 and [18.2](#). In [24] noisy corruptions were not considered and only the proof-of-concept demonstration of how the continuous nonlinear spectrum can be used for transmission was presented. The input pattern used for numerical calculations was built from the sequence of $N = 100$ of pulses and had the following form:

$$q(z = 0, t) = \sum_{k=1}^N c_k s(t - kT), \quad (18.20)$$

with T being the symbol duration ($T = T_s$). As an example, the quadrature phase shift keying modulation (QPSK) of the information coefficients was employed: The absolute value of $c_{\alpha k}$ is the same for each coefficient, $|c_k| = c = \text{const.}$, and the phase of each c_k takes four discrete values from the set:

$$\text{Arg}\{c_k\} = 2\pi p/4, \quad \text{with } p = 0 \div 3. \quad (18.21)$$

The whole set of c_k (18.21) can be rotated to an arbitrary angle in the complex plane. So, the constellation diagram of the input signal (the loci of c_k in the complex plane for all carrier numbers k) consists of four points. The value

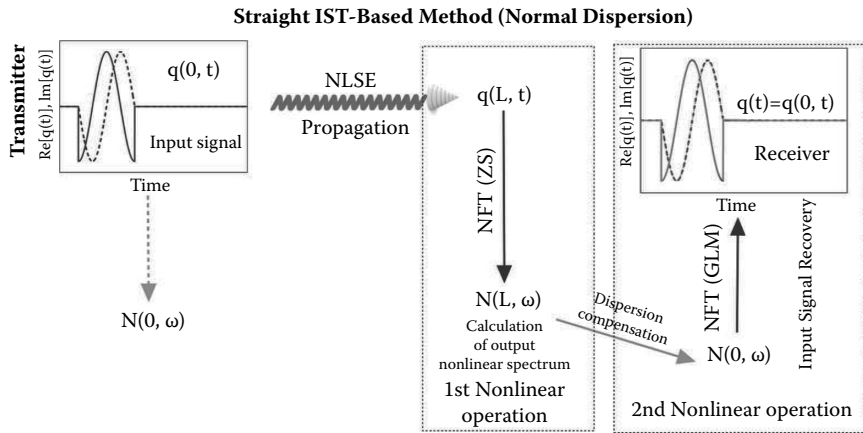


FIGURE 18.2: Flowchart of the transmission scheme for the straight IST-based nonlinearity compensation, utilized in [24] for the focusing NLSE.

$|c_k| = c = 0.5$ was taken, which produced observable nonlinear effects over distances ~ 1000 km. The input carrier pulse shape $f_0(t)$ can have an arbitrary profile, and in [24] a Gaussian pulse shape was chosen,

$$s(t) = \exp \left[-t^2 / (2\tau_0^2) \right] \times \exp [i\phi],$$

where parameter τ_0 is related to the pulse full width at half maximum width through $T_{FWHM} = 1.655 \tau_0$, and the phases were generated randomly from the QPSK set (18.21).

The transmission scheme considered in [24] is given in Fig. 18.2. The scheme involves two NFT operations, both at the receiver side. First, using the profile at the receiver, one inserts it into the FNFT associated with the focusing NLSE, Eq. (18.16), then unrolls the accumulated dispersion inside the nonlinear spectral domain, and finally recovers the profile using the BNFT operation given by the appropriate GLME (18.18). The results for the application of this scheme vs linear dispersion compensation, Fig. 18.1, to the received waveform emerging from the same input (18.20), were compared at different propagation distances on the eye diagrams, Fig. 18.3 (superposition of waveforms from different slots), and constellation diagrams (indicating the position of coefficients c_k on the complex plane), Fig. 18.4. When the absolute value of coefficients is small (low powers), the reconstructed signals for the linear and nonlinear methods are almost identical; reconstruction via the scheme from Fig. 18.1 is very quick and efficient. However, with an increase of nonlinearity, the FT approach becomes less efficient, whereas the NFT results change very little, mostly due to the increase in NFT computational errors. Figure 18.3 shows the eye diagrams of reconstructed signals for different distances, obtained by using both linear and nonlinear approaches. We can see that the IST (NFT)

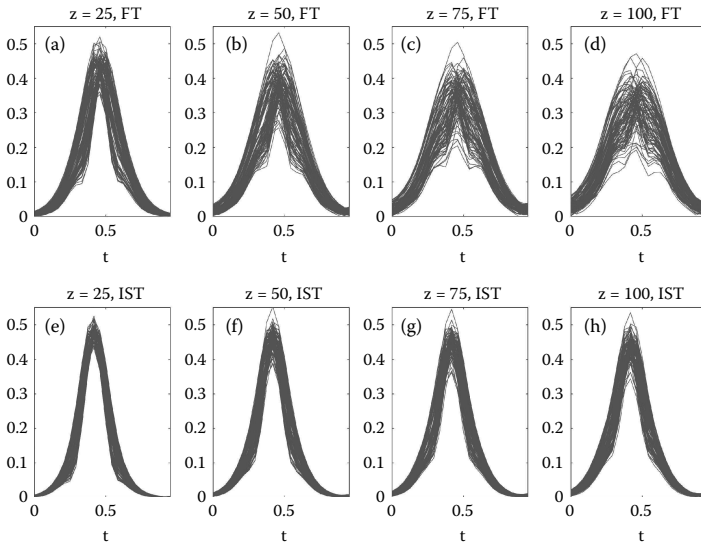


FIGURE 18.3: Eye diagram for the signals reconstructed via FT: (a) at $z = 25$; (b) at $z = 50$; (c) at $z = 75$; (d) at $z = 100$; and via IST: (e) at $z = 25$; (f) at $z = 50$; (g) at $z = 75$; (h) at $z = 100$. Taken from [24].

approach, Fig. 18.3(e–h), provides better results than the compensation via the FT, Fig. 18.3(a–d). With an increase of the propagation distance, the “eye” in Fig. 18.3(a–d) starts “closing,” while for the IST approach, the “eye” remains well open. Figure 18.4 shows the corresponding constellation diagrams for reconstructed signals, indicating the same tendency.

So, although nonlinear transmission impairments due to fiber Kerr nonlinearity can be compensated by the DBM method (see Subsection 18.2.4), it requires substantial computational efforts to model reverse signal channel propagation. The key technical difference between compensation of linear channel dispersion and nonlinear effects is that the linear Fourier transform compensates for accumulated channel dispersion analytically, without using any computer time for reverse propagation. The NFT-based scheme illustrated in this section allows one to do the same with nonlinear impairments. Of course, there is a price to pay for such an advantage, meaning that one has to deal with the NFT, instead of performing direct and inverse linear FT, as would be the case in linear channel equalization.

In conclusion, this section simply illustrates the recovery of a nonlinearly distorted signal using NFT-based signal processing. In this technique a propagation part is trivial and technical problems are moved to the receiver side. It has to be noted that the deviations of the waveform obtained with the use of the NFT from the initial ones, observable in Figs. 18.3 (e)–(h) and 18.4 (e)–(h), arise due to computational errors and periodic boundary conditions,

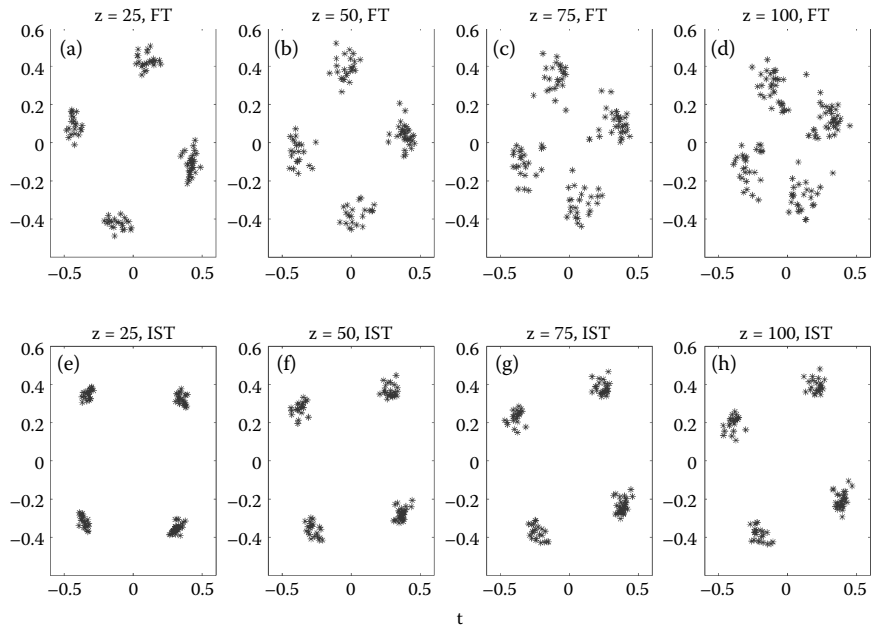


FIGURE 18.4: Constellation diagram for the signals reconstructed via FT: (a) at $z = 25$; (b) at $z = 50$; (c) at $z = 75$; (d) at $z = 100$; and via IST: (e) at $z = 25$; (f) at $z = 50$; (g) at $z = 75$; (h) at $z = 100$. Taken from [24].

used for the integration of the NLSE. When these factors are eliminated (or mitigated), the recovery of the profiles at the receiver side would become perfect.

18.4 METHOD OF NONLINEAR AND LINEAR SPECTRA EQUALIZATION FOR LOW ENERGY SIGNALS: ANOMALOUS DISPERSION

In this section we deal with the anomalous dispersion case and describe a straightforward method of linear and nonlinear spectra equalization [25], applicable in the case of weak power signals $|q(t)| \sim \varepsilon$ having a finite extent $[-T/2, T/2]$ (burst mode transmission). The method provides a good illustration of how the transition from linear to nonlinear quantities occurs. The low power condition implies that no solitons can form from our input, so that the ZSSP (18.5) does not contain discrete eigenspectrum: $\Sigma = [\rho(\xi), \xi \in \text{Re}]$, the *complete* set of scattering data (18.8) consists only of the quantity $\rho(\xi)$. The first question with regard to nonlinear spectrum manipulation is how one can encode nonlinear spectral data at the transmitter side and then retrieve

them at the receiver. Note that the results given in [Subsection 18.4.1](#) below are general and do not imply any specific modulation format. In fact, the only limitation of the method is the relative smallness of the input signal amplitude multiplied to the pulse duration.

18.4.1 NONLINEAR SPECTRUM EXPANSIONS FOR LOW SIGNAL AMPLITUDE

Using the smallness of ε we can obtain expressions for the nonlinear spectrum using perturbative iterations. We start from Eq. (18.5), looking for the solution expansion in terms of the parameter εT . First, in ZSSP (18.5) one makes the transformation from $\phi_{1,2}$ to slow varying functions $\varphi_{1,2}$ as $\varphi_{1,2} = e^{\mp i\xi t} \phi_{1,2}$. In terms of $\varphi_{1,2}$, the expression for $\rho(\xi)$ (18.7) now changes to

$$\rho(\xi) = \lim_{t \rightarrow \infty} \frac{\varphi_2(\xi, t)}{\varphi_1(\xi, t)}. \tag{18.22}$$

Solving the ZSSP recast in terms of $\varphi_{1,2}$ by recursive iterations gives us

$$\varphi_2(t, \xi) = - \int_{-T/2}^t dt_1 e^{-2i\xi t_1} \bar{q}(t_1) + \int_{-T/2}^t dt_1 \int_{-T/2}^{t_1} dt_2 \int_0^{t_2} dt_3 e^{2i\xi(t_2-t_1-t_3)} \bar{q}(t_1) q(t_2) \bar{q}(t_3),$$

up to ε^3 (each power of q gives the contribution $\sim \varepsilon$), and

$$\varphi_1(t, \xi) = 1 - \int_{-T/2}^t dt_1 \int_{-T/2}^{t_1} dt_2 e^{2i\xi(t_1-t_2)} q(t_1) \bar{q}(t_2),$$

up to ε^2 . The expression for $\rho(\xi)$ takes the form $\rho(\xi) \approx \rho_0(\xi) + \rho_1(\xi)$, where $\rho_0 \sim \varepsilon$ and $\rho_1 \sim \varepsilon^3$ are given as follows (the next term is $\sim \varepsilon^5$):

$$\rho_0(\xi) = - \int_{-T/2}^{T/2} dt_1 e^{-2i\xi t_1} \bar{q}(t_1), \tag{18.23}$$

$$\rho_1(\xi) = - \int_{-T/2}^{T/2} dt_1 \int_{t_1}^{T/2} dt_2 \int_{-T/2}^{t_2} dt_3 e^{2i\xi(t_2-t_1-t_3)} \bar{q}(t_1) q(t_2) \bar{q}(t_3). \tag{18.24}$$

Now we “propagate” our $\rho(\xi)$ to the distance L using Eq. (18.9),

$$\rho(L, \xi) = \rho_0(L, \xi) + \rho_1(L, \xi) = [\rho_0(\xi) + \rho_1(\xi)] e^{2i\xi^2 L}, \tag{18.25}$$

to obtain the expression for nonlinear spectral distribution at $z = L$, where $\rho_0(L, \xi) \sim \varepsilon$ and $\rho_1(L, \xi) \sim \varepsilon^3$.

18.4.2 LINEAR AND NONLINEAR SPECTRA EQUALIZATION USING SIGNAL PRE-DISTORTION

Suppose that at the input $z = 0$, we apply pre-distortion $s(t) \sim \varepsilon^3$ to the initial signal waveform $q(t)$:

$$q_s(t) = q(t) + s(t). \quad (18.26)$$

The idea of the method is to remove the quantity $\rho_1(\xi)$ given by Eq. (18.24) and thus the term $\rho_1(L, \xi)$ from the spectral density at the end point $z = L$ in Eq. (18.25), by using the additional pre-processing given by $s(t)$. When a small quantity $s(t) \sim \varepsilon^3$ is added to the input signal, one gains a correction $\rho_s(\xi) \sim \varepsilon^3$ to the expression for $\rho_1(\xi)$ (see Eq. (18.24)):

$$\begin{aligned} \rho(\xi) &= \rho_0(\xi) + \rho_1(\xi) + \rho_s(\xi) + O(\varepsilon^5), \\ \rho_s(\xi) &= - \int_{-T/2}^{T/2} dt_1 e^{-2i\xi t_1} \bar{s}(t_1). \end{aligned} \quad (18.27)$$

For the two terms of the same order, $\rho_1(\xi)$ and $\rho_s(\xi)$, to cancel each other, we choose $s(t)$ in such a way that the following relation is satisfied:

$$\rho_s(\xi) = -\rho_1(\xi). \quad (18.28)$$

Using the definition of the NSF (18.11), we can now obtain the ordinary Fourier spectrum $S(\omega)$ for our correction $s(t)$ as

$$S(\omega) = \bar{\rho}_1(\xi) \Big|_{\xi = -\frac{\omega}{2}}, \quad (18.29)$$

and performing the backward FT of Eq. (18.29), we restore the profile of $s(t)$ in the time domain. Thus, for the pre-distorted signal $q_s(t) = q(t) + s(t)$, with the FT of $s(t)$ given by Eq. (18.29), the addition to the nonlinear spectrum $\sim \varepsilon^3$ disappears altogether and *the nonlinear spectrum associated with $q_s(t)$ coincides with the linear spectrum of initial $q(t)$ up to the terms $\sim \varepsilon^5$.*

The flowchart of the pre-compensation scheme and the signal recovery at distance $z = L$ is given in Fig. 18.5. We note that, aside from recursive Fourier-type integration used to obtain $\rho_1(\xi)$, the scheme involves just one FNFT. So, by means of the pre-compensation described above, one is able to translate the encoded information into the nonlinear spectral domain without using any special formats, and control the accuracy of the data mapping. The transmission itself is effectively performed through the nonlinear spectral domain.

18.4.3 ILLUSTRATION OF THE METHOD

18.4.3.1 Optical frequency division multiplexing (OFDM) modulation

For the illustration of how the current and other methods work, as an example we consider input in the form of the burst-mode (several symbols of) OFDM. Generally, coherent optical OFDM has recently become a popular transmission technique owing to its robustness against chromatic and polarization mode dispersion, efficiency and practicality of implementation; see the monograph [49] and references therein. OFDM is a multi-carrier transmission format where a data stream is carried with many lower-rate tones:

$$q(t) = \sum_{\alpha=-\infty}^{\infty} \sum_{k=0}^{N_{sc}-1} c_{\alpha k} s_k(t - \alpha T) e^{i\Omega_k t}. \tag{18.30}$$

Here, $c_{\alpha k}$ is the α -th informational coefficient in the k -th subcarrier, s_k is the waveform of the k -th subcarrier, N_{sc} is the total number of subcarriers, Ω_k is the frequency of the k -th subcarrier, and T is the OFDM symbol (slot) duration. The shape of each subcarrier, $s_k(t)$, is usually a rectangle $\Pi(t)$ of width T and unit height, and such a choice ensures the orthogonality condition

$$\delta_{kl} = \frac{1}{T} \int_0^T s_k(t) \bar{s}_l(t) e^{i(\Omega_k - \Omega_l)t} dt,$$

which is met as long as the subcarrier frequencies satisfy $\Omega_k - \Omega_l = (2\pi/T)m$, with an integer m . This means that for linear transmission these orthogonal subcarrier sets, with their frequencies spaced at multiples of the inverse of

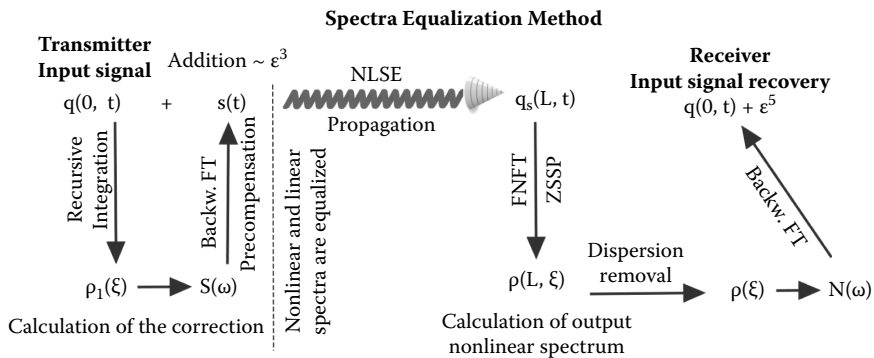


FIGURE 18.5: Flowchart of the pre-compensation scheme for the equalization of the linear and nonlinear spectra up to ϵ^5 and the subsequent recovery of the informational content at the receiver. Taken from [25].

the symbol rate, $\Omega_k = (2\pi/T)(k - 1)$, can be recovered without intercarrier (IC) and intersymbol (IS) interference, in spite of strong spectral signal overlapping. The coefficients $c_{\alpha k}$ are then recovered by a convolution with the appropriate conjugate base function $\bar{q}_{\alpha k} = \Pi(t)(t - \alpha T) e^{-i\Omega_k t}$. The linear spectrum of the OFDM-modulated signal (18.30) is a comb of sinc-like shapes:

$$Q(\omega) = 2 \sum_{\alpha=-\infty}^{\infty} \sum_{k=1}^{N_{sc}} c_{\alpha k} \exp[-i\omega\alpha T + (i/2)(\Omega_k - \omega)T] \frac{\sin\left[\frac{(\Omega_k - \omega)T}{2}\right]}{\Omega_k - \omega}. \quad (18.31)$$

18.4.3.2 Spectra equalization for OFDM input signals

18.4.3.2.1 Single OFDM tone

First, it is instructive to consider pre-distortion for the simple input in the form of a single OFDM tone $q(0, t) = c e^{i\Omega t}$ if $t \in [-\frac{T}{2}, \frac{T}{2}]$, and 0 otherwise, assuming its amplitude $|c| \sim \varepsilon \ll 1$ and using the results of [Subsection 18.4.2](#). The ZSSP for this input profile can be solved analytically [25], so the results of the expansion can be checked directly. The first-order term in the expansion of $\rho(\xi)$ (where the corresponding NSF coincides with the linear spectrum) is given by

$$\rho_0(\xi) = -\bar{c}_k \frac{\sin T(\xi + \Omega/2)}{\xi + \Omega/2}. \quad (18.32)$$

For the nonlinear addition $\sim \varepsilon^3$, we have

$$\rho_1(\xi) = 2\bar{c}_k |c_k|^2 \exp[i(\xi + \Omega/2)T] \frac{\sin T(2\xi + \Omega) - T(2\xi + \Omega)}{(\xi + \Omega/2)^3}. \quad (18.33)$$

Now, one calculates the pre-distortion spectrum $S(\omega)$, inserting (18.33) into Eqs. (18.28) and (18.29). The resulting function $s(t)$ is given in [Fig. 18.6\(b\)](#) for the case $T = 1$, $\varepsilon = 0.5$, $\Omega = 2\pi$ [see the profile of $q(t)$ in [Fig. 18.6\(a\)](#)]. Interestingly, the resulting profile of $s(t)$ is asymmetric with respect to the time axis origin, in contrast the obvious symmetry of the input pulse.

In [Fig. 18.6\(c\)](#), we present a comparison of the absolute errors for the linear scheme in [Fig. 18.1](#) and the error for the scheme from [Fig. 18.5](#). One observes that the resulting error for the equalization method is generally four to five times smaller compared to the case with linear dispersion compensation even for such a low power input. Note that the largest errors for the pre-distorted pulse occurred at the points $t = \pm T/2$, i.e., where there was a sharp change in the input profile. These errors are caused by numerical discretization aliasing.

18.4.3.2.2 Several OFDM symbols

For illustration purposes, in [25] the random QPSK encoding (18.21) of OFDM coefficients was adopted and the following normalizing parameters were used:

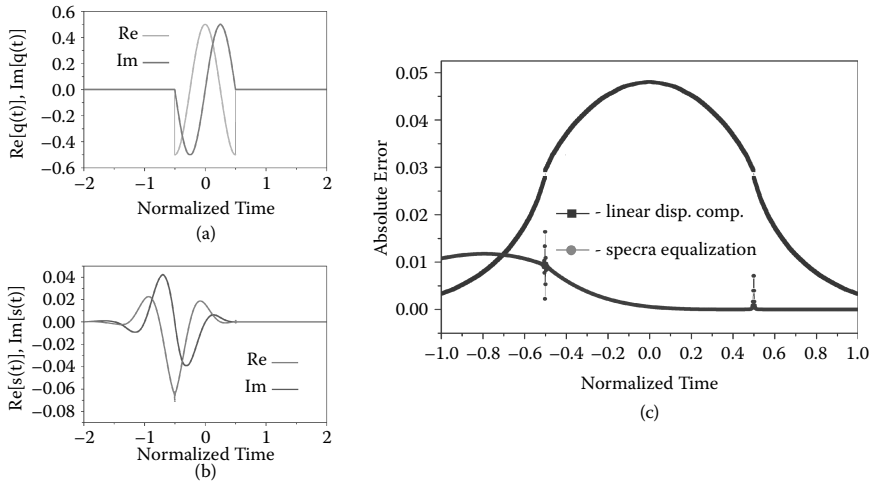


FIGURE 18.6: (a) Real and imaginary parts of the input profile corresponding to a single OFDM tone with $T = 1$. (b) Real and imaginary parts of the corresponding nonlinear pre-distortion profile $s(t) \sim \varepsilon^3$. (c) The absolute errors, obtained by the application of spectra equalization pre-compensation (circles) (see Fig. 18.5) and linear dispersion removal (squares) (see Fig. 18.1) at distance $z = 1$ ($L = 4000$ km). Taken from [25].

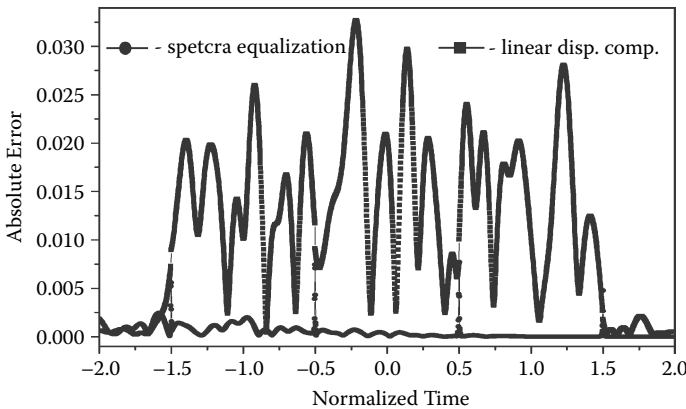


FIGURE 18.7: Absolute errors for the propagation of three slots (normalized duration of each slot $T = 1$) of the 10-mode QPSK-OFDM with $|c_{\alpha k}| = 0.15$, obtained by the application of spectra equalization pre-compensation (circles) (see Fig. 18.5) and linear dispersion removal (squares) (see Fig. 18.1) at distance $z = 1$. Taken from [25].

$T_s = 300$ ps, giving the characteristic z normalization scale as $Z_s \approx 4000$ km. The input pulse was taken as a finite number (a burst) of OFDM symbols (18.30), with 10 tones in each symbol. The ε^3 correction to $\rho(\xi)$ can also be obtained analytically [25] and contains contributions from both the IS and IC interference terms. The absolute errors associated with the propagation of the pre-compensated OFDM vs the errors produced by the linear dispersion compensation (Fig. 18.1) of the same OFDM sequence are summarized in Fig. 18.7. We can see that the pre-compensation error is still much lower than that of the linear method (notice the aliasing contribution at the ends of each slot) in spite of the extended total duration of the burst pulse (for the simulation in Fig. 18.7 three OFDM slots were used). In [25], the robustness of the method from Fig. 18.5 against ASE-induced noise was also checked, and simulations using the NLSE with a noise term (18.3) and realistic noise intensity were performed. It was shown that the presence of ASE does not violate the general performance of the transmission based on nonlinear spectrum evolution. The results for the NFFT-based method were better than those for the application of the simple linear scheme from Fig. 18.1.

18.5 NONLINEAR INVERSE SYNTHESIS (NIS) METHOD – ANOMALOUS DISPERSION

18.5.1 GENERAL IDEA OF THE METHOD

In the previous two sections the preliminary “proof-of-concept” demonstration that the non-solitonic part of the nonlinear spectrum can be used for mitigating nonlinear distortions was presented. However, these methods have limited applicability, being confined to the normal dispersion case or to the low-power initial signals. The method described in this section is rather more challenging and practically important, dealing with the focusing NLSE and high-power inputs [32, 33]. Note that, for an arbitrary high-energy input for the focusing NLSE, we usually have the formation of solitons [20, 21], and the eigenvalue spectrum of ZSSP, Eq. (18.5), contains complex eigenvalues corresponding to solitonic degrees of freedom (aside from highly disordered inputs [50, 51], which are less interesting in transmission problems). When the high-power input is randomly coded, the complex eigenvalue portrait of ZSSP can be extremely involved. It means that the implementation of the direct scheme given in Fig. 18.2 brings about considerable difficulties related to finding the location of eigenvalues and the recovery of a profile using the general form of the focusing GLME (18.18) with solitonic components (18.19). To get rid of this issue, we suggest *synthesizing* the profile in the time domain starting from given encoded shapes in the nonlinear spectral domain. In other words, one performs a one-to-one mapping of the linear spectrum $Q(\omega)$ for the known information-bearing signal $q(t)$ to the nonlinear spectrum (NSF) $N(\omega)$, where the latter already corresponds to a new signal $q_{GLM}(t)$: $Q(\omega) \rightarrow N(\omega)$. Then the new profile in the time domain $q_{GLM}(t)$ is synthesized using the BNFT,

i.e., by solving the GLME (18.18) and using the corresponding $N(\omega)$ (or $r(\xi)$, given by Eq. (18.14)). Notably, for high powers the synthesized signal $q_{GLM}(t)$ can be essentially different from the initial waveform $q(t)$. Such an encoding can explore the advantages of well-developed linear formats, like OFDM, as the propagation of the nonlinear spectrum is linear. The idea itself is similar to that widely used for the inverse syntheses of Bragg gratings [45, 47]: One creates the input profile bearing the desired properties, starting from the nonlinear spectral data, and then employs the BNFT, thus synthesizing the profile in the time domain. Because of this similarity we call this method “nonlinear inverse synthesis” (NIS) [32, 33]. During the evolution, the spectral data undergo just a trivial phase rotation without nonlinear mode coupling or channel crosstalk, and hence after winding out this “nonlinear dispersion” at the receiver, the initial information can be recovered without nonlinear signal degradation. The scheme of the NIS method is illustrated in Fig. 18.8. The NIS method involves two stages: (i) the BNFT at the transmitter, providing the profile $q_{GLM}(0, t)$ in the time domain corresponding to a desired initial NSF $N(\omega)$; and (ii) the recovery of the reflection coefficient and corresponding NSF at the receiver by the FNFT, i.e., by solving Eq. (18.5), and the consequent dispersion compensation inside the nonlinear spectral domain.

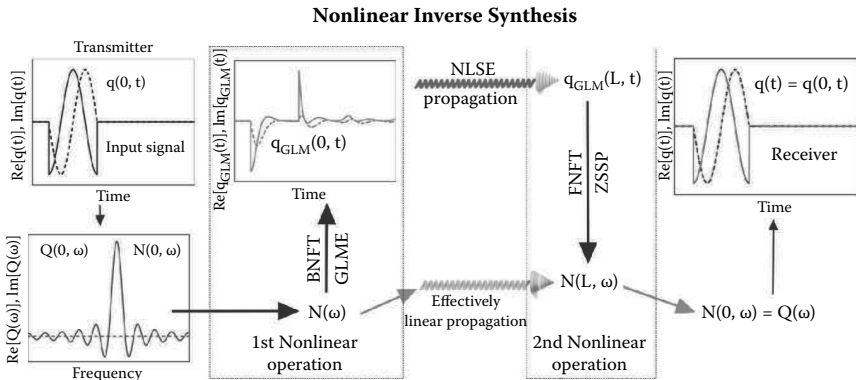


FIGURE 18.8: Flowchart depicting the sequence of operations for the NIS method, the example initial waveform $q(0, t) = e^{2\pi it/T}$ if $t \in [0, T]$, 0 otherwise. The panes display the true profiles for $T = 1$ ns, transmission length $L = 2000$ km (noiseless case). Taken from [32].

Downloaded by [Aston University] at 01:44 14 December 2016

18.5.2 ILLUSTRATION OF THE METHOD

18.5.2.1 Synthesis of profiles from some characteristic shapes in the nonlinear spectral domain

The first question of interest with respect to NIS method implementation is: What do the elementary base functions look like in the time domain when its spectral shape is used in the nonlinear spectral domain? We present the corresponding results in Fig. 18.9. Figure 18.9(a) and (b) show the results for the sinc base (i.e., it is a rectangle with amplitude c in the ω domain) taken as an NSF. This type of base function is utilized in the Nyquist-format technique, which provides the highest spectral efficiency. As seen from Fig. 18.9(b), the corresponding profiles in the time domain, $q_{GLM}(t)$, are not symmetric, and the asymmetry grows with the increase of amplitude c . In the OFDM scheme the elementary base in the time domain is simply a rectangle, i.e., a sinc-function in the ω -domain. The inverse NFFT of the single OFDM spectral tone, $N(\omega) = c \text{sinc}(\omega)$, is given in Fig. 18.9(c) and (d) for different values of amplitude c .

We see that for a sufficiently large c the waveform of $q_{GLM}(t)$ is significantly different from a rectangular profile occurring in the linear case: While losing its symmetry, the profile develops an oscillatory advancing tail. The general form of the spectrum of an arbitrary OFDM-encoded data sequence is given by Eq. (18.31). In Figs. 18.9(e) and (f) we present the spectrum of a single OFDM slot containing 10 subcarriers with $c_k = 1$ and a corresponding inverse NFFT, $q_{GLM}(t)$. (The general form of the spectrum of an arbitrary OFDM-encoded data sequence is given by Eq. (18.31).) In this case the structure of the advancing tail is more involved and reflects the structure of the pulse itself.

18.5.2.2 NIS for high-efficiency OFDM transmission – Comparison with digital backpropagation

In [33] 56 Gbaud OFDM NIS-based transmission systems (in burst mode) with different modulation formats were studied: In addition to the QPSK, the higher level quadrature amplitude modulations 16QAM (16 possible complex values for c_k), and 64QAM (64 possible values) of the OFDM coefficients were used. The net data rates of these systems, after removing overhead, were 100 Gb/s, 200 Gb/s, and 300 Gb/s, respectively. The guard time duration is chosen as 20 percent longer than the fiber chromatic dispersion induced memory for a 2000 km link. For the OFDM NIS-based system, the total number of tones was 128, where 112 subcarriers were filled with data, while the remaining subcarriers were set to zero. The useful OFDM symbol duration was 2 ns and the cyclic prefix was not used. Each packet data (burst) contained only one OFDM symbol (slot).

The linear spectra of OFDM signals before and after the BNFT are shown in the Fig. 18.10. It can be seen that after the BNFT, the linear spectrum

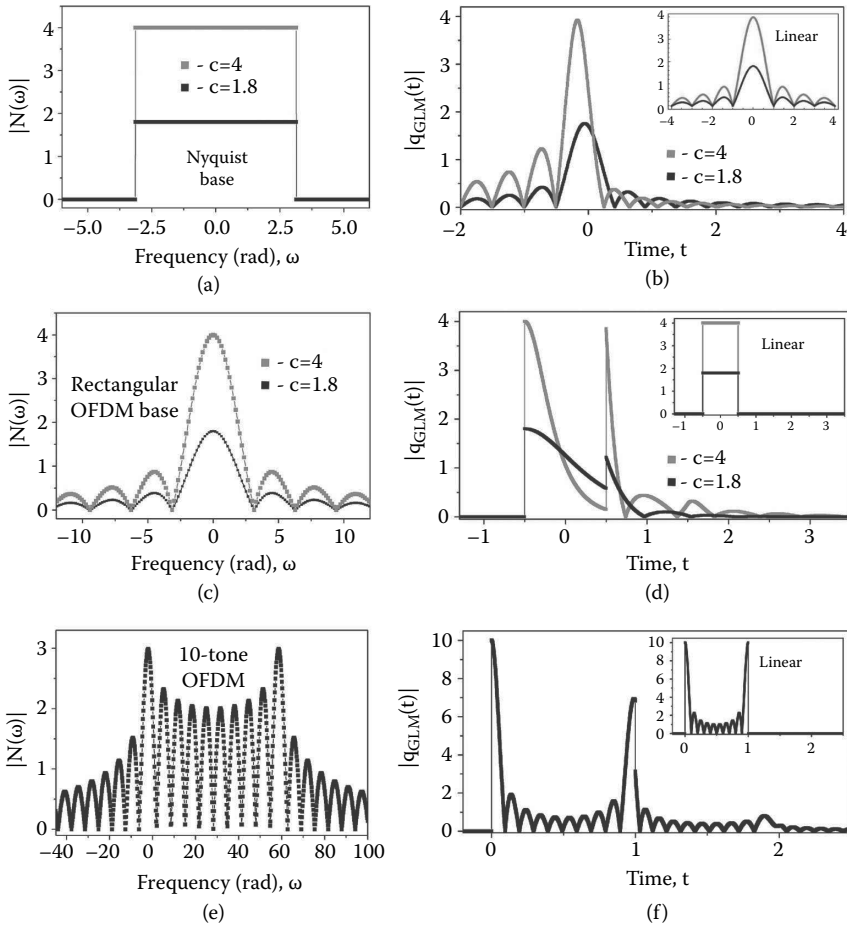


FIGURE 18.9: Profiles of NSF $|N(\omega)|$ with different amplitudes and the corresponding profiles $|q_{GLM}(t)|$ in the time domain, obtained by solving GLME Eq. (18.18). (a), (b) For the rectangle-shaped $N(\omega) = \prod(\omega/2\pi)$; (c), (d) for the sinc-shaped $N(\omega)$ (the base of standard OFDM); (e), (f) $N(\omega)$ and corresponding $q_{GLM}(t)$ for a single slot of 10 OFDM tones, with $c_k = c = 1$. The insets show the corresponding linear FTs of the spectrum. Taken from [32].

of the OFDM signal does not broaden significantly, indicating that the NIS method combined with the OFDM can be effectively applied for a WDM transmission or even multiplexed into superchannels.

In [33] the Q-factor (calculated through the error vector magnitude; see [52]) for the evaluation of the OFDM coefficient deviations was chosen as the performance indicator for the transmission quality assessment. In Fig. 18.11 the information recovery for the NIS method is again compared with the

linear dispersion compensation, Fig. 18.1; for the NIS, the Q-factor for the back-to-back (B2B) recovery with no propagation and after the propagation for 2000 km is presented. Noise was not included for the simulations given in Fig. 18.11, so that fiber nonlinearity was the only impairment. This result confirms that the NIS-based approach can perfectly compensate for the deterministic impairment due to fiber nonlinearity, using just a single-tap linear dispersion removal for the nonlinear spectrum at the receiver. However, one can notice that the back-to-back performance of NIS-based systems deteriorates when the input signal power increases. This phenomenon can be explained by the fact that the numerical error of both FNFT and BNFTs grows with the increase of input signal power [33].

Now we compare the performance of the OFDM systems with the use of the NIS and DBP methods [35] (see Subsection 18.2.4) for fiber nonlinearity compensation. For the implementation of DBP, the received signal is first filtered with an eighth order low-pass filter having a bandwidth of 40 GHz. Subsequently, the optical field is reconstructed and the signal is back-propagated with a different number of steps per single span, indicating the numerical complexity of the corresponding DBP realization. In Fig. 18.12 we compare the Q-factors of OFDM systems with NIS and DBP. One can see that the OFDM NIS-based system offers over 3.5 dB advantage over the traditional OFDM system, confirming the effectiveness of the proposed approach for fiber nonlinearity compensation. This performance improvement is comparable with that of DBP with 10 steps per span. The launch power in the NIS-based system is limited to -4 dBm (the optimum launch power), which is mainly due to numerical errors in the NFT operations at the transmitter and receiver.

When combining it with a higher modulation format, such as 16QAM, the OFDM NIS-based approach offers nearly 4 dB advantage over the traditional OFDM scheme; see Fig. 18.13. The transmission bit rate in this case is

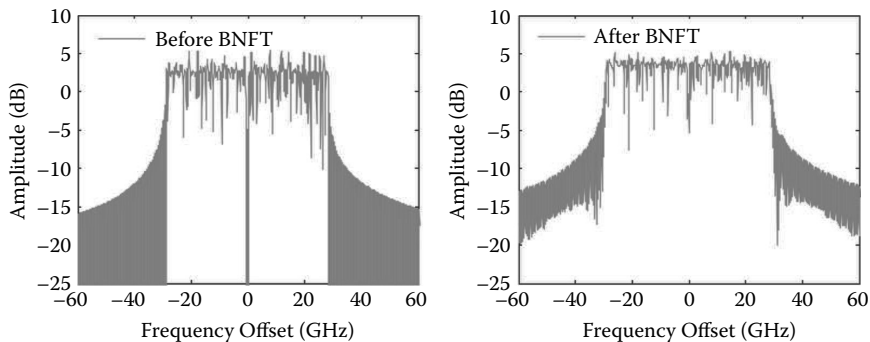


FIGURE 18.10: Linear spectra of 128-tone randomly coded QPSK-OFDM signals before and after BNFT; the launch power is 0 dBm. Taken from [33].

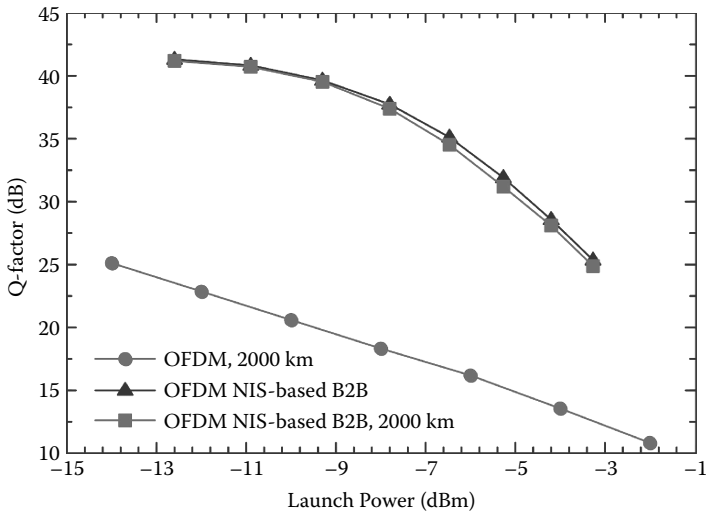


FIGURE 18.11: Q-factor as a function of launch power for linear dispersion removal, Fig. 18.1, and for a 100 Gb/s QPSK-OFDM NIS-based system without ASE-induced noise. Taken from [33].

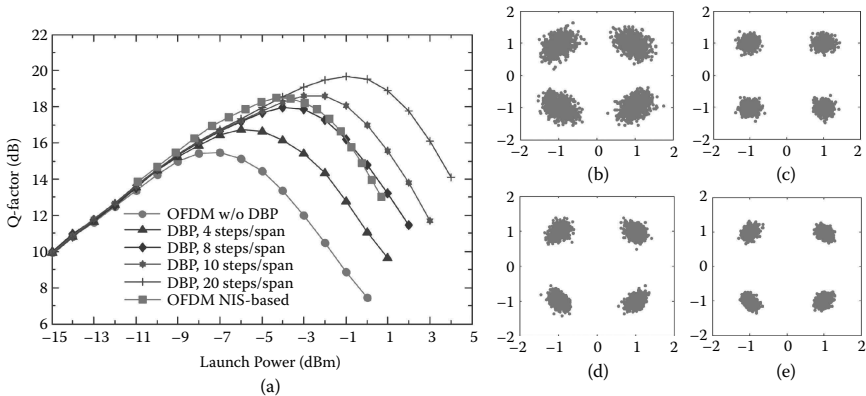


FIGURE 18.12: (a) Performance comparison of 100-Gb/s QPSK-OFDM systems with the NIS vs. the DBP methods for fiber nonlinearity compensation. The receiver filter bandwidth used was 40 GHz; the distance is 2000 km. The right panels show constellation diagrams at the optimum launch powers with and without the NIS and DBP methods for fiber compensation: (b) without NIS and DBP, (c) with the NIS method, (d) DBP with 10 steps/span, (e) DBP with 20 steps/span. Taken from [33].

Downloaded by [Aston University] at 01:44 14 December 2016

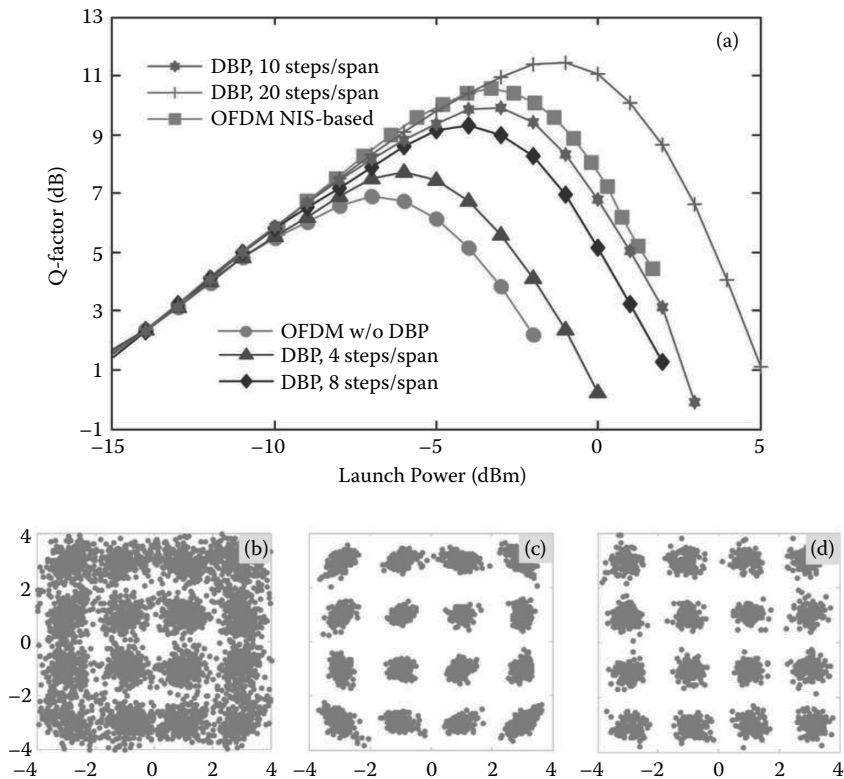


FIGURE 18.13: (a) Performance comparison of the 200-Gb/s 16QAM-OFDM systems with the NIS vs. the DBP methods for fiber nonlinearity compensation. The receiver filter bandwidth used was 40 GHz; the distance is 2000 km. The right panels show constellation diagrams at the optimum launch powers with and without the NIS and DBP methods for fiber compensation: (b) without NIS and DBP, (c) DBP with 20 steps/span, (d) with the NIS method. Taken from [33].

200 Gb/s. It can be seen that for the 16QAM modulation format, the OFDM NIS-based system outperforms the DBP with 10 steps per span. The optimum constellation diagrams for the conventional OFDM system, OFDM NIS-based, and OFDM with 20 steps per span DBP are shown in Fig. 18.13(b)–(d). From this figure one can observe that the NIS method produced fairly clear constellation diagrams. The simulation results for the 300-Gb/s 64QAM OFDM NIS-based system are compared in Fig. 18.14 with the conventional OFDM and OFDM with DBP. It can be seen that for such a high-order modulation format, the OFDM NIS-based system displays almost the same performance as the DBP with 20 steps per span. The performance improvement in compar-

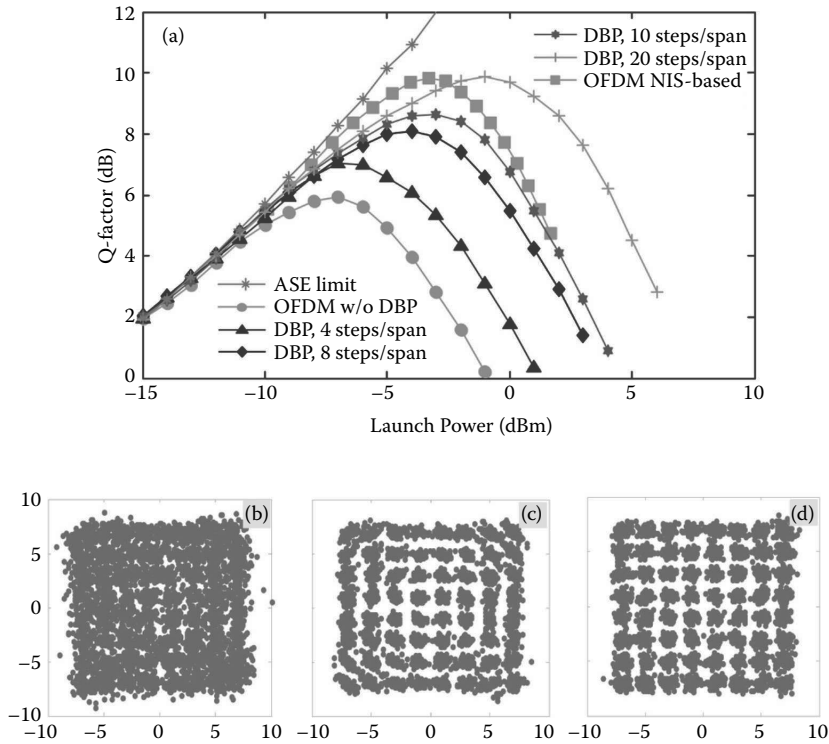


FIGURE 18.14: The same as in Fig. 18.13 but for the 300-Gb/s 64QAM-OFDM systems. Taken from [33].

Comparison with the conventional OFDM system is about 4.5 dB, which is larger than the values achieved for the QPSK and 16QAM modulation formats. This result indicates that a greater performance advantage of the OFDM NIS-based system over the traditional approaches can be reached for higher-order modulation formats and shows the considerable benefit of the NIS method for fiber nonlinearity compensation for highly spectrally efficient transmission systems. In Fig. 18.14 the curve indicating the ASE transmission limit is also presented: For calculating it, nonlinearity was completely removed. It can be seen that the curve for the NIS-based transmission generally goes above those for the DBP in the noise-dominated region, but it does not intersect the limiting line. This behavior reveals that the NIS-based transmission is less sensitive to noise-induced corruption than the DBP, and the refinements of the NFT processing techniques can improve the NIS performance even further.

To sum up, the NIS method can be successfully combined with the transmission techniques (e.g., OFDM, Nyquist-shaped) having high spectral efficiency and advanced modulation formats, such as QPSK, 16QAM, and 64QAM. This novel transmission scheme suggests encoding the information

onto the continuous part of the nonlinear spectrum and requires only single-tap equalization at the receiver to compensate for all the deterministic fiber nonlinearity impairments accumulated along the fiber link. Generally, the NIS concept can be further extended to other optical systems described by different integrable continuous equations. The simulations confirmed the effectiveness of the NIS scheme and showed that an improvement of 4.5 dB can be achieved, which is comparable to the multi-steps per span DBP compensation method. With the utilization of increasingly higher-order modulations (16- and 64QAM), the results for the performance of the NIS-based OFDM system became comparable with the performance of increasingly higher-order DBP compensation (i.e., with progressively more steps per span). This fact reveals that the NIS method efficiency can become strongly competitive and outperform that of the DBP methods for high spectral efficiency formats. In [33] the performance of the Nyquist-shaped modulation format combined with the NIS method was also studied, and it was demonstrated that the OFDM is potentially a more suitable modulation for such systems.

18.6 CONCLUSION

In this chapter we have reviewed recent progress in the promising re-emerging communication technique based on transmission using the continuous part of the nonlinear spectrum associated with an integrable evolutionary equation, in particular, with the NLSE (18.1). This bevy of methods is a ramification the original idea of Hasegawa and Nyu [15], the “eigenvalue communication,” where the data are encoded onto the parameters of specifically nonlinear “normal modes” and thus are not affected by nonlinear impairments during transmission. So, the major advantage of using the nonlinear spectral domain for data transmission in a coherent communication channel is a suppression of nonlinear cross-talk insofar as the fiber nonlinearity is effectively included into the digital signal processing based on NFT operations. The resulting channel becomes effectively linear, and the signal propagation boils down to the trivial phase rotation of individual (nonlinear) spectral components. This allows us to employ well-developed modulation formats, recasting them into the nonlinear spectral domain. Also, the robustness of NFT-based transmission in a practical environment that includes ASE noise was demonstrated. For the most advanced and practically attractive recently introduced NIS method (Section 18.5), it was shown that an improvement (in terms of the Q-factor) of 4.5 dB can be achieved, which is comparable to that for the multi-steps per span DBP compensation method. In addition, NFT-based processing can be competitive and even outperform that of the “traditional” digital signal processing methods, like DBP, with the use of recent advances in NFT processing methods [46, 48].

In a recent work of Buelow [34] the important first experimental evidence that nonlinear spectral data can be used for optical transmission was presented. In this experimental work, signal detection based on NFT process-

ing in a coherent receiver was assessed: 16 GBaud binary phase-shift keying (BPSK) signals were transmitted over a few spans of standard single-mode fiber at power levels which induce a strong nonlinear distortion. The detection scheme employed the discrete (multi-soliton) eigenvalues of the ZSSP. The experimental work [34] clearly indicates that NFT-based detection can be applied in practical fiber optic systems.

The concept of eigenvalue communication is re-emerging as a powerful nonlinear digital signal processing technique that paves the way to overcoming current limitations of traditional communications methods in nonlinear fiber channels. Its methodology is not ultimately linked to the NLSE model considered in this chapter but can be further extended to other communication systems described by other integrable evolutionary equations, with the most important example being the Manakov system of equations [22], governing the transmission of a polarization multiplexed optical signal. This means that the technique considered here can be further developed and generalized to the case of polarization division multiplexing systems. The other important direction in the progress of these methods is to develop and optimize modulation formats specifically for coding of the signal inside the nonlinear spectral domain, aiming at an increase of the spectral efficiency and performance improvement with regard to the signal corruptions occurring due to the deviation of the real channel from a purely integrable model. In particular, the experiments of Buelow [34] indicate that the channel performance evaluation with regard to the EDFA-based system with strong attenuation has to be addressed. A no less important area is the further development of superfast numerical methods for NFT-based processing, i.e., the development of fast NFT processing algorithms. Finally, we strongly believe that the two current practical implementations of the “eigenvalue communication,” namely, transmission based on the discrete (solitonic) part of the spectrum and transmission techniques using the continuous spectrum part, will eventually merge together, thus emanating into a single, solid, highly efficacious and extremely flexible nonlinear digital signal processing technique. Numerous aspects of the fundamental IST method are available for integration into communication engineering technologies, and we hope that the ideas of the NFT become no less common and routine for optical engineers than the standard linear Fourier operations are now. This requires efforts from different research communities and serves as a remarkable example of the groundbreaking impact that interdisciplinary research can produce.

ACKNOWLEDGMENTS

The work has been supported by EPSRC project UNLOC EP/J017582/1. The support of the Russian Ministry of Education and Science and the European Research Council project ULTRALASER is also acknowledged. We would like to thank all our colleagues who have participated in the research and contributed to the results described in this review chapter.

REFERENCES

1. R. Essiambre, G. Kramer, P. J. Winzer, G. J. Foschini, and B. Goebel. Capacity limits of optical fiber networks. *Journal of Lightwave Technology*, 28(4):662–701, 2010.
2. A. D. Ellis, J. Zhao, and D. Cotter. Approaching the non-linear Shannon limit. *Journal of Lightwave Technology*, 28(4):423–433, 2010.
3. D. J. Richardson. Filling the light pipe. *Science*, 330(6002):327–328, 2010.
4. R. I. Killey and C. Behrens. Shannon's theory in nonlinear systems. *Journal of Modern Optics*, 58(1):1–10, 2011.
5. A. Hasegawa and F. Tappert. Transmission of stationary nonlinear optical pulses in dispersive dielectric fibers. 1. Anomalous dispersion. *Applied Physics Letters*, 23(3):142–144, 1973.
6. G. P. Agrawal. *Fiber-Optic Communication Systems*, 4th ed. John Wiley & Sons, Inc., Hoboken, NJ, 2010.
7. A. Hasegawa and Y. Kodama. *Solitons in Optical Communications*. Clarendon Press, Oxford, 1995.
8. L. F. Mollenauer and J. P. Gordon. *Solitons in Optical Fibers: Fundamentals and Applications*. Academic Press, San Diego, 2006.
9. M. Nakazawa, H. Kubota, K. Suzuki, and E. Yamada. Recent progress on soliton transmission technology. *Chaos*, 10(3):486–513, 2000.
10. S. K. Turitsyn, B. Bale, and M. P. Fedoruk. Dispersion-managed solitons in fiber systems and lasers. *Physics Reports*, 521(4):135–203, 2012.
11. S. K. Turitsyn, E. G. Shapiro, S. B. Medvedev, M. P. Fedoruk, and V. K. Mezentsev. Physics and mathematics of dispersion-managed optical solitons. *Comptes Rendus Physique* 4(1):145–161, 2003.
12. J. E. Prilepsky, S. A. Derevyanko, and S. K. Turitsyn. Temporal solitonic crystals and non-Hermitian informational lattices. *Physical Review Letters*, 108(187), art. no 183902, 2012.
13. O. Yushko, A. Redyuk, M. Fedoruk et al. Timing and phase jitter suppression in coherent soliton transmission. *Optics Letters*, 39(21):6308–6311, 2014.
14. O. V. Yushko and A. A. Redyuk. Soliton communication lines based on spectrally efficient modulation formats. *Quantum Electronics*, 44(6):606–611, 2014.
15. A. Hasegawa and T. Nyu. Eigenvalue communication. *Journal of Lightwave Technology*, 11(3):395–399, 1993.
16. V. E. Zakharov and A. B. Shabat. Exact theory of two-dimensional self-focusing and one-dimensional self-modulation of waves in nonlinear media. *Soviet Physics-JETP*, 34(1):62–69, 1972.
17. M. J. Ablowitz, D. J. Kaup, A. C. Newell, and H. Segur. The inverse scattering transform-Fourier analysis for nonlinear problems. *Studies in Applied Mathematics*, 53(4):249–315, 1974.
18. A. R. Osborne. The inverse scattering transform: tools for the nonlinear Fourier analysis and filtering of ocean surface waves. *Chaos, Solitons & Fractals*, 5(12):2623–2637, 1995.
19. A. S. Fokas and I. M. Gelfand. Integrability of linear and nonlinear evolution equations and the associated nonlinear Fourier transforms. *Letters in Mathematical Physics*, 32(3):189–210, 1994.
20. V. E. Zakharov, S. V. Manakov, S. P. Novikov, and L. P. Pitaevskii. *Theory of Solitons. The Inverse Scattering Method*. Consultants Bureau, New York, 1984.

21. M. J. Ablowitz and H. Segur. *Solitons and the Inverse Scattering Transform*. SIAM, Philadelphia, 1981.
22. S. V. Manakov. On the theory of two-dimensional stationary self focussing of electromagnetic waves. *Soviet Physics-JETP*, 38(2):248–253, 1974.
23. S. Oda, A. Maruta, and K. Kitayama. All-optical quantization scheme based on fiber nonlinearity. *IEEE Photonics Technology Letters*, 16(2):587–589, 2004.
24. E. G. Turitsyna and S. K. Turitsyn. Digital signal processing based on inverse scattering transform. *Optics Letters*, 38(20):4186–4188, 2013.
25. J. E. Prilepsky, S. A. Derevyanko, and S. K. Turitsyn. Nonlinear spectral management: Linearization of the lossless fiber channel. *Optics Express*, 21(20):24344–24367, 2013.
26. H. Terauchi and A. Maruta. Eigenvalue modulated optical transmission system based on digital coherent technology. In *18th OptoElectronics and Communications Conference held jointly with 2013 International Conference on Photonics in Switching (OECC/PS)*, paper WR2-5. IEICE, 2013.
27. M. I. Yousefi and F. R. Kschischang. Information transmission using the nonlinear Fourier transform, Part I: Mathematical tools. *IEEE Transactions on Information Theory*, 60(7):4312–4328, 2014.
28. M. I. Yousefi and F. R. Kschischang. Information transmission using the nonlinear Fourier transform, Part II: Numerical methods. *IEEE Transactions on Information Theory*, 60(7):4329–4345, 2014.
29. M. I. Yousefi and F. R. Kschischang. Information transmission using the nonlinear Fourier transform, Part III: Spectrum modulation. *IEEE Transactions on Information Theory*, 60(7):4346–4369, 2014.
30. H. Terauchi, Y. Matsuda, A. Toyota, and A. Maruta. Noise tolerance of eigenvalue modulated optical transmission system based on digital coherent technology. In *2014 OptoElectronics and Communication Conference and Australian Conference on Optical Fiber Technology*, pages 778–780. Engineers Australia, 2014.
31. S. Hari, F. Kschischang, and M. Yousefi. Multi-eigenvalue communication via the nonlinear Fourier transform. In *27th Biennial Symposium on Communications (QBSC)*, pages 92–95. IEEE, 2014.
32. J. E. Prilepsky, S. A. Derevyanko, K. J. Blow, I. Gabitov, and S. K. Turitsyn. Nonlinear inverse synthesis and eigenvalue division multiplexing in optical fiber channels. *Physical Review Letters*, 113(1), art. no. 013901, 2014.
33. S. T. Le, J. E. Prilepsky, and S. K. Turitsyn. Nonlinear inverse synthesis for high spectral efficiency transmission in optical fibers. *Optics Express*, 22(22):26720–26741, 2014.
34. H. Buelow. Experimental assessment of nonlinear Fourier transformation based detection under fiber nonlinearity. In *European Conference on Optical Communications*, paper We.2.3.2, 2014.
35. E. Ip and J. M. Kahn. Compensation of dispersion and nonlinear impairments using digital backpropagation. *Journal of Lightwave Technology*, 26(20):3416–3425, 2008.
36. S. L. Jansen, D. Van den Borne, B. Spinnler et al. Optical phase conjugation for ultra long-haul phase-shift-keyed transmission. *Journal of Lightwave Technology*, 24(1):54–64, 2006.

37. X. Liu, A. R. Chraplyvy, P. J. Winzer, R. W. Tkach, and S. Chandrasekhar. Phase-conjugated twin waves for communication beyond the Kerr nonlinearity limit. *Nature Photonics*, 7(7):560–568, 2013.
38. J. D. Ania-Castanon. Quasi-lossless transmission using second-order Raman amplification and fiber Bragg gratings. *Optics Express*, 12(19):4372–4377, 2004.
39. J. D. Ania-Castanon, T. J. Ellingham, R. Ibbotson, X. Chen, L. Zhang, and S. K. Turitsyn. Ultralong Raman fiber lasers as virtually lossless optical media. *Physical Review Letters*, 96(2), art. no. 023902, 2006.
40. T. J. Ellingham, J. D. Ania-Castanon, R. Ibbotson, X. Chen, L. Zhang, and S. K. Turitsyn. Quasi-lossless optical links for broad-band transmission and data processing. *IEEE Photonics Technology Letters*, 18(1):268–270, 2006.
41. J. D. Ania-Castanon, V. Karalekas, P. Harper, and S. K. Turitsyn. Simultaneous spatial and spectral transparency in ultralong fiber lasers. *Physical Review Letters*, 101(12), art. no 123903, 2008.
42. J. D. Ania-Castanon and S. K. Turitsyn. Unrepeated transmission through ultra-long fiber laser cavities. *Optics Communications*, 281(23):5760–5763, 2008.
43. G. Boffetta and A. R. Osborne. Computation of the direct scattering transform for the nonlinear Schrödinger equation. *Journal of Computational Physics*, 102(2):252–264, 1992.
44. S. Burtsev, R. Camassa, and I. Timofeyev. Numerical algorithms for the direct spectral transform with applications to nonlinear Schrödinger type systems. *Journal of Computational Physics* 147(1):166–186, 1998.
45. A. Buryak, J. Bland-Hawthorn, and V. Steblina. Comparison of inverse scattering algorithms for designing ultrabroadband fiber bragg gratings. *Optics Express*, 17(3):1995–2004, 2009.
46. S. Wahls and H. V. Poor. Introducing the fast nonlinear Fourier transform. In *Proceedings of IEEE International Conference on Acoustics, Speech, and Signal Processing (ICASSP)*, pages 5780–5784. IEEE, 2013.
47. O. V. Belai, L. L. Frumin, E. V. Podivilov, and D. A. Shapiro. Efficient numerical method of the fiber Bragg grating synthesis. *Journal of Optical Society of America B*, 24(7):1451–1457, 2007.
48. S. Wahls and H. V. Poor. Inverse nonlinear Fourier transforms via interpolation: The Ablowitz-Ladik case. In *Proceeding of International Symposium on Mathematical Theory of Networks and Systems (MTNS)*, pages 1848–1855, 2014.
49. S. Shieh and I. Djordjevic. *Orthogonal Frequency Division Multiplexing for Optical Communications*. Academic Press, Amsterdam, 2010.
50. S. A. Derevyanko and J. E. Prilepsky. Random input problem for the nonlinear Schrödinger equation. *Physical Review E*, 78(4), art. no 046610, 2008.
51. S. K. Turitsyn and S. A. Derevyanko. Soliton-based discriminator of noncoherent optical pulses. *Physical Review A*, 78(6), art. no 063819, 2008.
52. S. T. Le, K. J. Blow, V. K. Menzentssev, and S. K. Turitsyn. Comparison of numerical bit error rate estimation methods in 112 Gbs QPSK CO-OFDM transmission. In *39th European Conference and Exhibition on Optical Communication (ECOC)*, paper P4.14. 2013.